Correlations between structural properties and performance of microcrystalline silicon solar cells fabricated by conventional RF-PECVD

Liwei Li [a], Yuan-Min Li [b], J.A. Anna Selvan [b], Alan E. Delahoy [b], Roland A. Levy [a],*

[a] *Department of Physics, New Jersey Institute of Technology, 323 King Boulevard, Newark, NJ 07102, USA*
[b] *Energy Photovoltaics, Inc., 276 Bakers Basin Road, Lawrenceville, NJ 08648, USA*

Abstract

In this study, direct structural characterization of μc-Si:H solar cells deposited by conventional RF-PECVD was conducted using Raman spectroscopy, XRD, and AFM. Strong correlations between i-layer structural properties and device performance were established. A wide variety of i-layer microstructures, from mixed-phase Si:H to highly crystalline μc-Si:H, were revealed by Raman scattering. Micro-crystallinity obtained from Raman scattering, presented as I_c/I_a, proved to be sensitive to the microstructure of μc-Si:H i-layers. Strong spatial non-uniformity of i-layer microstructure as well as variations in device performance were observed. It has been demonstrated here that stable, high performance μc-Si:H solar cells can only be obtained with i-layers being μc-Si:H, yet close to the μc-Si:H to mixed-phase Si:H transition edge where an optimum micro-crystallinity range (I_c/I_a at around 1.8) was identified. It was shown by XRD experiments that high performance, optimum μc-Si:H solar cells exhibit smaller grain sizes compared to solar cells with i-layers showing higher micro-crystallinity. Correlations among non-uniformity pattern, i-layer micro-crystallinity, and AFM surface morphologies were also observed.
© 2004 Elsevier B.V. All rights reserved.

PACS: 81.05.Gc; 81.07.Bc; 81.10.Aj; 81.15.Gh

1. Introduction

Over the past few years, solar cells with hydrogenated microcrystalline silicon (μc-Si:H) intrinsic (i-)layers have attracted extensive attention due to their demonstrated high stability under light soaking and successful application as the narrower-bandgap component in tandem photovoltaic (PV) devices [1–3]. Structural characterization has shown that μc-Si:H is a highly complex material which can take on a variety of microstructures and exhibit very different qualities depending on the exact deposition conditions. Unlike amorphous silicon (α-Si:H), which can be grown readily on various substrates, μc-Si:H and performance of μc-Si:H based solar cells are highly affected by the nature and surface morphology of substrates, reactor geometries, as well as the processing sequences [4–7]. Generally, stand-alone films (rather than devices) deposited on special substrates (e.g., Corning 7059 glass, etc.) are used to characterize α-Si:H. In the case of μc-Si:H, however, properties obtained from stand-alone films may not be necessarily translated into the μc-Si:H i-layer incorporated within actual p–i–n device configurations. Some other issues recently revealed such as the effect of accumulated bulk layer thickness on the growth of μc-Si:H, non-uniformity during μc-Si:H deposition, and narrow optimum processing windows

for high quality μc-Si:H [8–11], enhance the necessity of direct structural characterization of μc-Si:H solar cells, which is relatively lacking.

This study focuses on direct structural characterization of μc-Si:H p–i–n solar cells fabricated using a low cost, large-area RF-PECVD system [8]. While reducing the possibility of misinterpretation, direct structural characterization limits the application of some experimental techniques requiring special substrates and sample structures. Thus, only Raman spectroscopy, X-ray diffraction (XRD), and atomic force microscopy (AFM) were primarily used in this research for structural characterization of μc-Si:H solar cells. By means of direct structural characterization, correlations between i-layer structural properties and device performance of μc-Si:H solar cells were systematically investigated though understandings on the microscopic mechanisms of μc-Si:H growth and its effect on the performance of μc-Si:H solar cells are hindered by the complexities of μc-Si:H resulting from harsh deposition conditions.

2. Experimental

Single junction p–i–n type solar cells with μc-Si:H i-layers were deposited on commercial grade SnO_2/soda-lime-glass superstrates at low temperatures (near 200 °C) by glow discharge of highly hydrogen diluted silane in a single chamber, non-loadlocked conventional RF-PECVD system which is capable of simultaneously coating four plates equal in size of $15'' \times 12''$. A layer of sputtered Al, without any rear reflectors, was used as standard back contacts. Device fabrication and performance testing, including $I–V$ characteristics, quantum efficiency (QE), and accelerated light soaking, were carried out at Energy Photovoltaics, Inc. (EPV). The accelerated light soaking was conducted under light intensity simulating 47 suns. The total light soaking time for each sample is 300 s which has been confirmed using α-Si:H solar cells to be long enough to produce light-induced degradation as the saturated degradation produced by conventional light soaking (simulating one sun) for hundreds of hours. Selected light soaking samples were annealed at 150 °C for 1 h.

Structural characterization, using Raman scattering, XRD, and AFM, were conducted directly on actual solar cells at New Jersey Institute of Technology (NJIT). Strong red-light spectral response (QE at 800 nm or longer) and Raman shift at about 520 cm^{-1} were taken as signatures of μc-Si:H. Raman scattering was performed with 830 nm diode laser excitation such that deep penetration can be achieved to probe the overall micro-crystallinity of the Si:H absorber layer (response is not confined to the surface layer). The unavoidable contributions from substrates, i-layer texture, and doped

layers, as well as large variations of optical absorption with i-layer properties, may introduce systematic errors. Thus, we prefer presenting the overall micro-crystallinity in terms of the ratio of peak intensities (I_c/I_a) of Raman shift corresponding to μc-Si:H (I_c) and α-Si:H (I_a) rather than deduction of crystalline volume fraction. The latter method is more commonly adopted by other groups. A Rigaku D/MAX-B XRD system and a Nanoscope IIIa AFM system were used to study film microstructures and surface morphologies of the Si:H (including μc-Si:H) solar cells. Generally, XRD signals from μc-Si:H solar cells are very weak and the SnO_2 substrates show strong contribution. Though the grain sizes were calculated using Scherrer formula, the results are usually inaccurate and inconsistent due to low signal to noise ratio. They are used to illustrate the relationship between device performance and i-layer microstructure, rather than accurately determine real grain sizes. Device thickness was measured using a Dektak IIIa stylus profilometer. The i-layer thickness was estimated by subtracting the thickness of doped layers which could be empirically determined from deposition conditions. Compared to the i-layer, the doped layers are very thin; the errors for calculating the i-layer thickness are estimated to be within 2%.

3. Results

3.1. Raman spectroscopy and non-uniformity of μc-Si:H solar cells

Since both doped p- and n-layers are very thin compared to i-layers, Raman spectra measured on μc-Si:H solar cells are mainly determined by i-layer microstructure. A wide variety of Raman spectra were observed depending on i-layer microstructure. For highly crystalline μc-Si:H i-layer, a sharp peak at around 520 cm^{-1} was observed. Both the 480 and 520 cm^{-1} peaks, representing the amorphous and crystalline constituents of Raman scattering, respectively, can coexist in the Raman spectrum when the i-layer is mixed-phase (α + μc)-Si:H. When the i-layer takes on a microstructure with little fraction of μc-Si:H crystallites embedded in α-Si:H matrix, only a slight shoulder appears at around 520 cm^{-1}. All these patterns, in reference to that of typical α-Si:H solar cell, are illustrated in Fig. 1. As previously mentioned, rather than deducting crystalline volume fraction, the micro-crystallinity of μc-Si:H i-layer is presented in terms of I_c/I_a which has proven to be very sensitive to i-layer microstructure change. The I_c/I_a values listed in the subfigures of Fig. 1 clearly quantitate the corresponding overall micro-crystallinity qualitatively revealed by the Raman spectra patterns.

Strong spatial non-uniformity over the $12'' \times 15''$ substrates, in all aspects including surface texture,
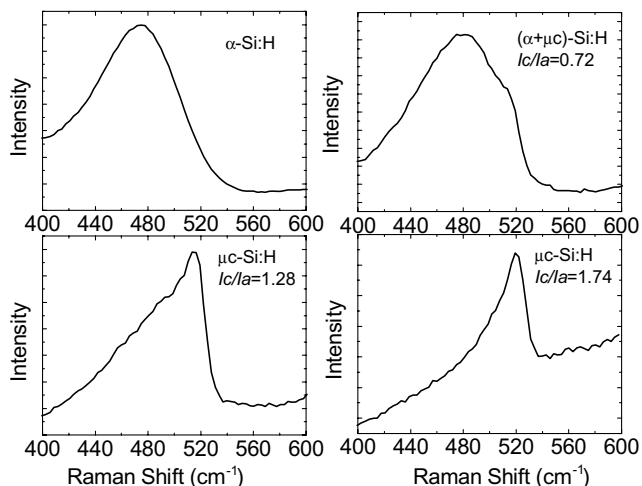
Fig. 1. Raman spectra of solar cells with various i-layers.

Fig. 2. Micro-crystallinity and device performance of μc-Si:H solar cells as functions of position. (a) Micro-crystallinity and efficiency; and (b) device performance parameters.

thickness, i-layer microstructure, and device performance, was observed from μc-Si:H solar cells. The microstructure and thickness non-uniformity patterns can even be easily detected by visual check. Looking through the p-layer side, areas with α-Si:H or mixed-phase Si:H i-layer appear dark red and areas with μc-Si:H i-layer show light red or orange colors. Within areas with similar microstructure, the visual color becomes lighter when the thickness decreases. Usually two types of non-uniformity over entire plate can be observed: (1) film thickness gradually decreases from the gas inlet side to the gas exhaust side over the substrates; (2) a highly hazy patch with milky color appears in the part close to gas inlet side while the area apart from the patch shows dull, specular look. Such structural non-uniformity was revealed clearly by Raman microcrystallinity. As illustrated in Fig. 2, a mixed-phase Si:H area, which precisely corresponds to the patch depicted above, is identified by I_c/I_a. Other regions on the plate exhibit much higher micro-crystallinity. Generally, the spatial non-uniformity exists along with the gas flow direction and good uniformity is usually obtained on the other direction.

Sharp changes, in both micro-crystallinity and device performance, occur at the two edges of the patch where strong phase transitions are revealed by Raman scattering. Compared to solar cells with μc-Si:H i-layers, devices with mixed-phase Si:H i-layers (inside the patch in this case) show higher open-circuit voltage (V_{oc}), lower short-circuit current density (J_{sc}), and lower fill factor (FF). However, the best solar cells are obtained at an 'optimum' region which is in highly crystalline region, yet close to the edge of microcrystalline to mixed-phase Si:H transition. Solar cells made from the area near gas exhaust showing even higher micro-crystallinity, or the area near the gas inlet, exhibit very low V_{oc}, low red-light response, and low conversion efficiencies, which is contrary to the assumption that highly crystalline μc-Si:H i-layers will generate more carriers at long wavelength light excitation and lead to strong red-light response.
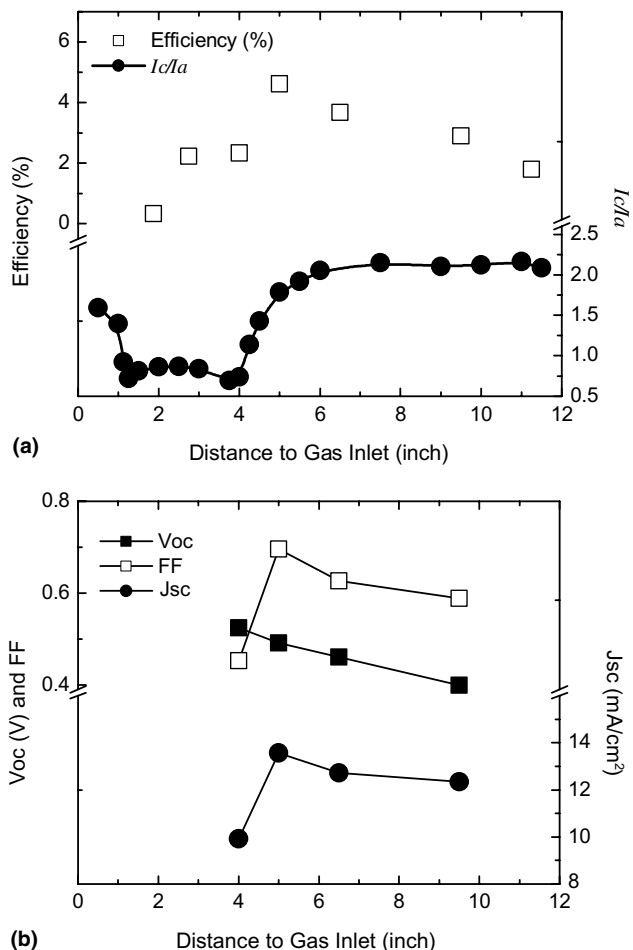
3.2. X-ray diffraction

Typical XRD spectra of μc-Si:H solar cells with various i-layer micro-crystallinity are shown in Fig. 3. XRD peaks at 2θ around 28.5°, 47.4°, and 56.2° were taken as signatures of Si(1 1 1), Si(2 2 0), and Si(3 1 1) planes, respectively. For most samples, Si(3 1 1) peaks are always very weak, if not undetectable. Compared to Raman scattering, XRD is less sensitive to the existence of μc-Si:H in the form of mixed-phase Si:H. No Si peaks are detected by XRD even though weak signal at $520\,cm^{-1}$, i.e., a slight shoulder, can be seen in corresponding Raman spectra. Fig. 4 shows the crystallographic texture, i.e., preferential crystal growth orientation, and grain sizes of μc-Si:H solar cells made from a plate exhibiting the 'patch' non-uniformity pat-
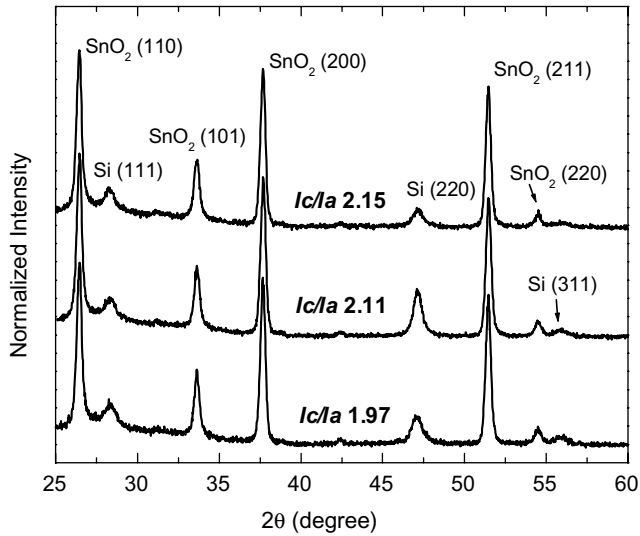
Fig. 3. XRD spectra of μc-Si:H solar cells with various i-layer micro-crystallinity.
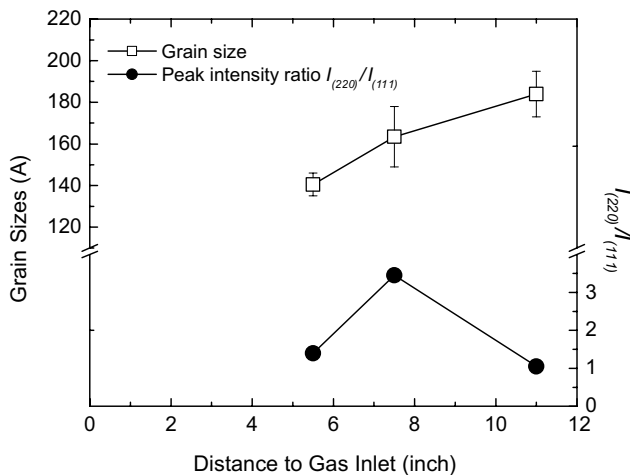
Fig. 4. Grain sizes and preferential crystalline orientation of μc-Si:H solar cells as functions of position.

tern as revealed in Fig. 2. The average of the grain sizes calculated from Si(1 1 1) and Si(2 2 0) peaks respectively was used in Fig. 4. The errors shown in Fig. 4 mainly came from the low signal to noise ratio due to strong contributions from SnO₂ substrate. Under normal geometrical conditions of $\theta - 2\theta$ scan, only those planes parallel to the sample surface will contribute to constructive interference. Therefore, the preferential orientation, i.e., the preferential piling up direction of the crystal planes during μc-Si:H growth, is presented by the peak intensity ratio of Si(2 2 0) and Si(1 1 1), denoted as $I_{(220)}$, and $I_{(111)}$, respectively.

It is evident from Fig. 2 and Fig. 4 that the optimal μc-Si:H solar cell made from materials near the μc-Si:H to mixed-phase Si:H transition edge shows smaller grain size and a little preferential growth along Si(2 2 0) compared to that made from near gas exhaust materials exhibiting higher micro-crystallinity. It can also be observed that, for μc-Si:H solar cells with good or fairly well performance, the conversion efficiencies decrease with increasing grain sizes, which agrees to the report from other groups [12]. Such decrease results from all the three major performance parameters, i.e., V_{oc}, J_{sc}, and FF.

Compared to standard XRD pattern of synthesized crystalline Si which exhibits a $I_{(220)}/I_{(111)}$ ratio of 0.55, μc-Si:H deposited in this study always shows Si(2 2 0) preferential growth. Unlike grain sizes, however, the change of preferential orientation does not show a pleasantly steady ascending or descending tendency. Crystal grains and grain boundaries are generally considered to strongly affect carrier transport. It is not clear what role is played by the preferential crystalline orientation of the film. While it has been shown that preferential growth strongly depends on plasma conditions, and the competition between selective etching and growth has been proposed as the growth kinetics of favorable crystal directions [13–15], detailed and precise mechanism remains elusive.

3.3. Atomic force microscopy

The AFM surface morphologies of solar cells with mixed-phase Si:H, near edge μc-Si:H, and highly crystalline μc-Si:H i-layers are shown in Fig. 5. The surface roughness (RMS, root means square) taken from AFM is plotted against device position and micro-crystallinity in Fig. 6. The effect of doped n-layer covering i-layer is estimated to be little since the n-layer is uniformly deposited over entire substrate and its thickness is much less than the height of surface clusters observed in AFM surface morphologies. From the edge of the non-uniformity patch (Fig. 5(a)) to the area near gas exhaust (Fig. 5(d)), the film thickness decreases from about 1.5 μm to 1.0 μm. The effect of such a thickness inhomogeneity on the AFM morphologies and surface roughness is of little concern since all samples have comparable thickness. The corresponding device performance and crystallographic results obtained from XRD can be found in Figs. 2 and 4, respectively.

Good correlations among visual non-uniformity pattern, micro-crystallinity, AFM morphologies, and surface roughness were observed. The sample made from the edge of non-uniformity patch (Fig. 5(a)), featuring sharp, large clusters unevenly distributed across the scanning area, shows the highest RMS surface roughness among all samples. Its surface roughness can even be observed visually by its highly hazy, milky color appearance. The area right in the middle of the non-uniformity patch (Fig. 5(b)) also shows large clusters but their heights and sharpness are much less than that
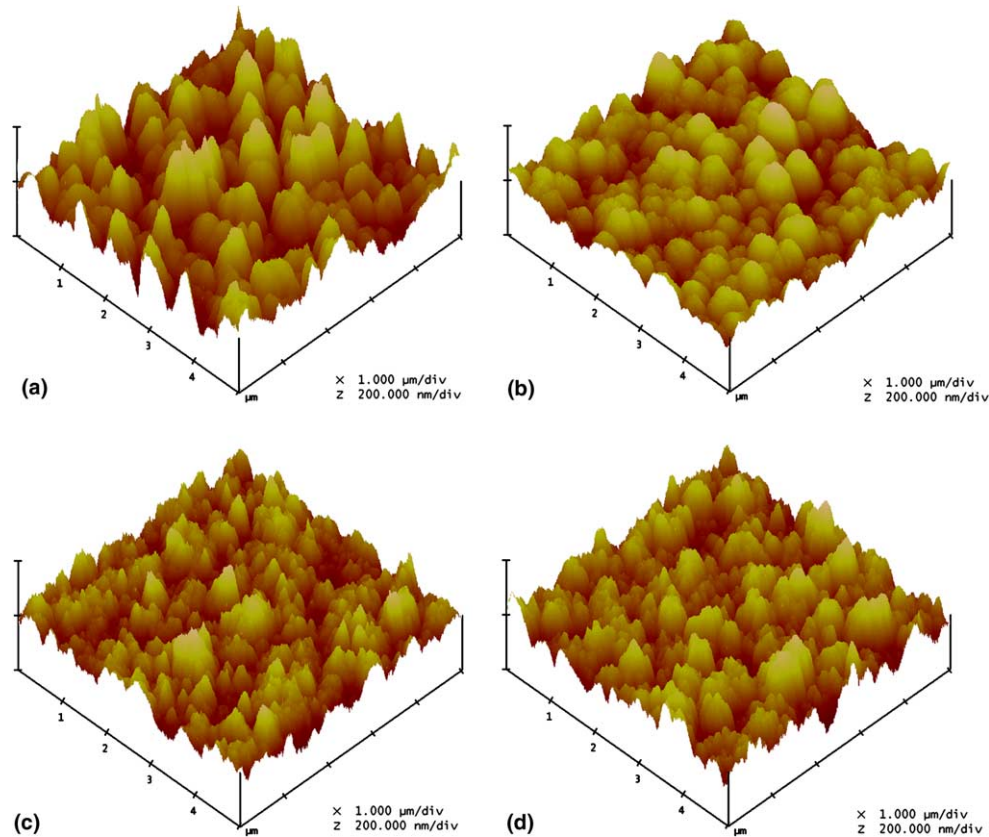
Fig. 5. AFM morphologies of μc-Si:H solar cells with various micro-crystallinity: (a) $I_c/I_a = 0.72$, RMS = 48.7 nm; (b) $I_c/I_a = 0.87$, RMS = 28.2 nm; (c) $I_c/I_a = 1.97$, RMS = 29.4 nm; and (d) $I_c/I_a = 2.15$, RMS = 34.8 nm.
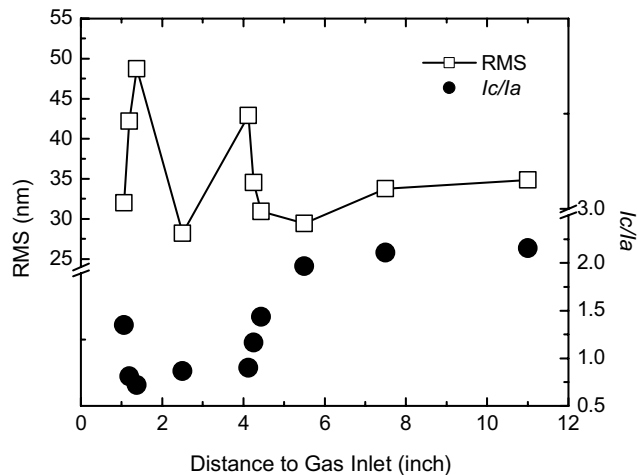
Fig. 6. Micro-crystallinity and surface roughness of μc-Si:H solar cells as functions of position.

shown in Fig. 5(a), leading to the lowest RMS surface roughness among all samples. Compared to all other samples, its surface morphology is also relatively regular. Surface morphologies of the optimum edge and highly crystalline areas close to the gas exhaust are shown in Fig. 5(c) and (d), respectively. All these surface morphologies exhibit comparable RMS surface roughness and similar features, i.e., numerous small clusters with some large aggregates distributed among them. The major difference of surface morphologies between the optimum edge area and more crystalline areas is that the amount of large aggregates increases with increasing micro-crystallinity (closer to gas exhaust).

4. Discussion

4.1. Non-uniformity of μc-Si:H solar cells

The non-uniformity features are mainly resulting from the gas flow pattern inside the reaction chamber which leads to non-uniform hydrogen dilution profile across the substrates under high plasma excitation. Generally, the uniformity tends to get worse with increasing growth rate (adjusted by plasma power) and silane depletion. When measured under negative bias, performance of those inferior solar cells made from mixed-phase Si:H or highly crystalline region can be significantly improved, indicating that carrier collection is highly suppressed in those areas. While it could be easily speculated that such suppression in highly crystalline area might be resulting from defects created by highly si-

lane depleted plasma, the suppression of carrier collection observed in the mixed-phase Si:H area, where the concentration of Si precursors (i.e., SiHx species) is supposed to be high enough to sustain the growth of mixed-phase Si:H, cannot be straightforwardly related to defects creation by hydrogen rich plasma.

Compared to mixed-phase Si:H area, μc-Si:H areas show less regular surface morphologies with smaller feature sizes (Fig. 5). The optimum edge area, where the highest performance devices are made, shows smallest surface feature (cluster) sizes. The non-uniform distribution of local SiHx concentration during μc-Si:H deposition is surely the major cause of the non-uniformity discussed above. If the columnar growth model by far proposed based on hydrogen dilution ratio [11,16,17] represents the real scenario, the AFM morphologies might imply, though highly speculative, some correlations between the surface morphologies and μc-Si:H growth process. In the areas where sufficient Si precursors are supplied during i-layer deposition, e.g., the middle of the patch, surface morphology similar to that of α-Si:H samples is observed (Fig. 5(b)). In the highly crystalline area, competitive growth among μc-Si:H crystallites results in small crystal clusters and coalescence of some clusters forms large aggregates, which are possibly responsible for the preferential growth orientation as well. At areas near gas exhaust, enhanced silane depletion results in stronger grain coalescence, leading to more large aggregates. The change of grain sizes against sample positions on the substrates obtained from XRD measurement, shown in Fig. 4, agrees to the above assumption. Stronger grain coalescence occurred near the gas exhaust area not only leads to larger grain sizes, but also leads to relatively higher RMS roughness as shown in Fig. 6, which agrees to the surface roughness change deduced from real time spectroscopic ellipsometry [18].

However, no clues are obtained so far by direct structural characterization pertaining to what happens at the strong phase transition edges, how the crystallographic texture (preferential orientation) forms, how the grain sizes and crystallographic texture affect the device performance, etc. Though basic understandings on these questions are sorely needed, it is very difficult to get direct evidence in view of the complexity taken on by μc-Si:H materials deposited using complicated seeding processes and i-layer deposition conditions.

4.2. Correlations between micro-crystallinity and device performance

Strong correlations between device performance and i-layer micro-crystallinity (I_c/I_a) were observed when the performance parameters of solar cells are plotted as functions of micro-crystallinity regardless of sample position and deposition conditions. From Figs. 7 and 8, it can be found that solar cells with mixed-phase Si:H i-layers ex-
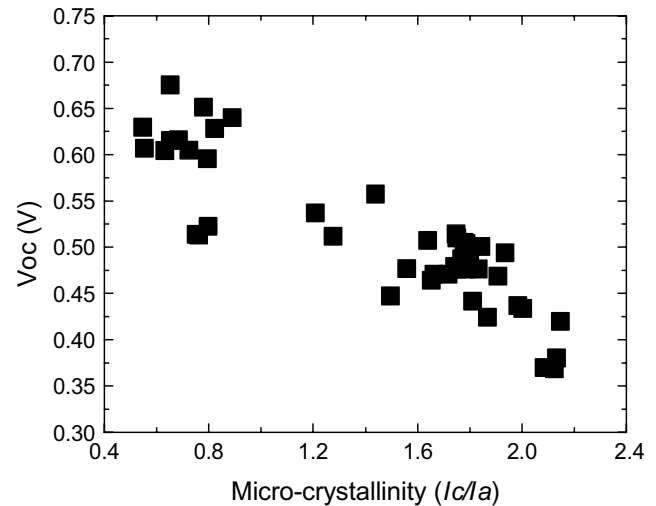
Fig. 7. V_{oc} as a function of micro-crystallinity.

hibit high V_{oc} and low red-light response while solar cells with μc-Si:H i-layers show low V_{oc} and high red-light response. Similar relationships between Raman micro-crystallinity and V_{oc} are also reported with μc-Si:H solar cells deposited using VHF-PECVD and Hot-wire CVD [19,20]. Though the red-light response measured without bias is rather scattered at high I_c/I_a, the tendency mentioned above is much enhanced when the QE are measured under −3 V bias as shown in Fig. 8. In either case, the highest red-light response is obtained at a narrow optimum I_c/I_a range (around 1.8) where V_{oc} of about 0.5 V or slightly lower is found. Actually, this I_c/I_a range exactly corresponds to the optimum μc-Si:H to mixed-phase Si:H transition 'edge' identified by structural characterization. The relationships between I_c/I_a and efficiencies, shown in Fig. 9, are more severely affected by de-
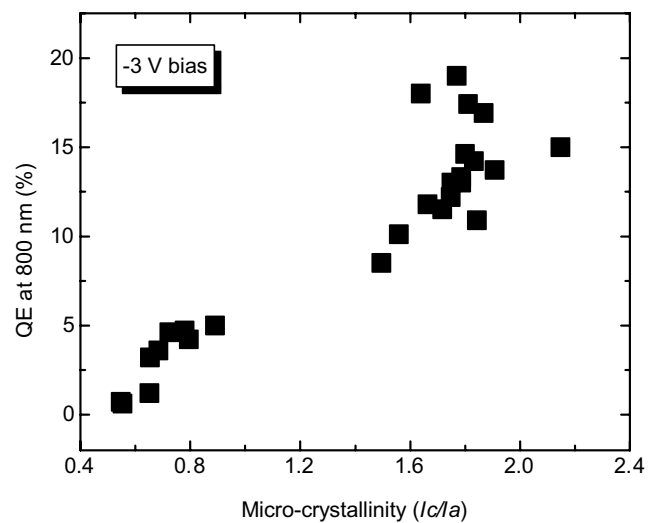
Fig. 8. Red-light response under −3 V bias as a function of micro-crystallinity.
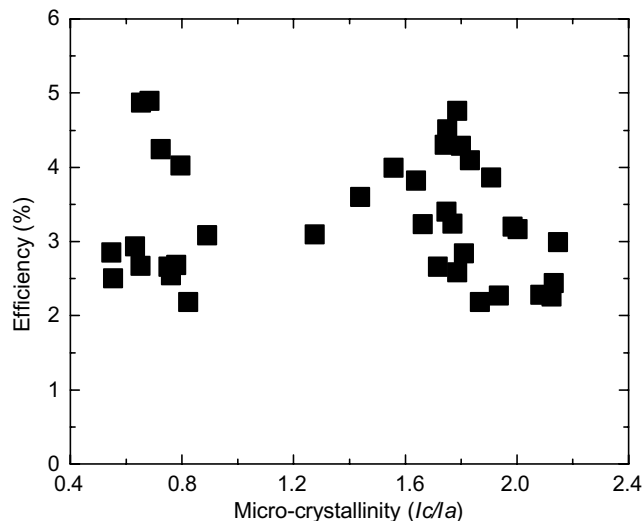
Fig. 9. Efficiency as a function of micro-crystallinity.

fects created by hydrogen rich plasma conditions than V_{oc} and red-light response and the data are rather scattered. However, the highest efficiencies are also obtained at the optimum I_c/I_a range identified in Figs. 7 and 8. Though very high initial efficiencies can be obtained at very low I_c/I_a value, such mixed-phase Si:H solar cells suffer from severe light-induced degradation, even worse than typical α-Si:H solar cells, as confirmed by Fig. 10. Both FF and J_{sc} exhibit similar features as that of efficiency vs. I_c/I_a with the highest FF and J_{sc} found at the optimum I_c/I_a. Generally, gradual decrease of the i-layer thickness from the optimum 'edge' to higher crystalline area (closer to gas exhaust) leads to lower J_{sc} for μc-Si:H solar cells with higher micro-crystallinity. However, the decrease of efficiencies for μc-Si:H solar cells, as shown in Fig. 9, results from not only the decrease of
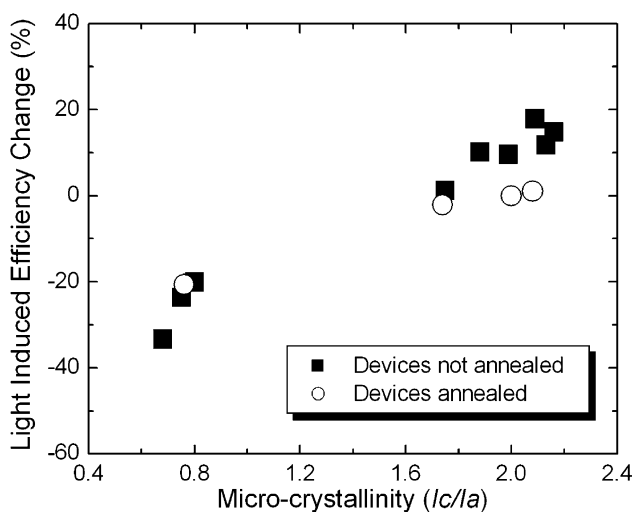
Fig. 10. Light-induced efficiency change under accelerated light soaking as a function of micro-crystallinity.

J_{sc} but also V_{oc} and FF as illustrated in Fig. 2(b) in which the film thickness (from the optimum 'edge' to gas exhaust) is about 1.4 μm, 1.2 μm, and 1.0 μm, respectively. The lower FF of the thinner, more crystalline solar cells, as compared to that of the optimum μc-Si:H solar cells, implies severer suppression of carrier collection in those devices. In Fig. 10 which illustrates the results of accelerated light soaking, light-induced efficiency increases are observed in un-annealed highly crystalline solar cells. However, such increases are significantly reduced once the solar cells are annealed before accelerated light soaking, indicating the existence of unstable defects in as-grown μc-Si:H solar cells.

As discussed above, μc-Si:H solar cells with both high initial and stabilized efficiencies can only be obtained at a very narrow optimum micro-crystallinity range, i.e., I_c/I_a at around 1.8, which precisely corresponds to the optimal μc-Si:H to mixed-phase Si:H transition edge as revealed by structural characterization. Compared to μc-Si:H solar cells with higher I_c/I_a, the optimum 'edge' μc-Si:H solar cells also show smaller grain sizes. However, reasons responsible for the deteriorated performance of solar cells with higher micro-crystallinity remain unclear. While breakdown of the internal electric field within thinner, highly crystalline μc-Si:H i-layers could be one reason, the possible causes may mostly relate to the relatively large grain boundaries in the highly crystalline areas which could form defective channels with more efficient contamination (contaminant precipitation), higher defect density, and less effective hydrogen passivation of dangling bonds in or near grain boundaries. These defects may not only result in recombination losses but also weaken the internal electric field (if defects exist near p/i interface), leading to even poorer carrier collection.

The optimum 'edge' identifies a very narrow optimum processing window for high quality μc-Si:H i-layers, i.e., μc-Si:H solar cells with high initial and stabilized efficiencies can only be obtained under deposition conditions which can produce μc-Si:H i-layers with the optimum micro-crystallinity. This issue, joined by the spatial non-uniformity of i-layer microstructure and device performance, present the major challenges in depositing high performance μc-Si:H solar cells in a low cost, large-area RF-PECVD system. While the non-uniformity can be improved by modify reactor geometries and gas flow patterns, the narrow optimum processing window, mainly affected by the local SiHx concentrations under high plasma power and high silane depletion conditions, must be addressed with extensive efforts in the future to develop low cost, high efficiency μc-Si:H solar cells.

5. Conclusions

Direct structural characterization of μc-Si:H solar cells was conducted using Raman scattering, XRD,

and AFM. A wide variety of i-layer microstructures, from mixed-phase Si:H to highly crystalline μc-Si:H, were revealed by Raman scattering. It was shown by XRD experiments that high performance, optimum μc-Si:H solar cells exhibit smaller grain sizes compared to solar cells with i-layers showing higher micro-crystallinity. Correlations among non-uniformity pattern, i-layer micro-crystallinity, XRD crystallographic characteristics, and AFM surface morphologies were observed.

Micro-crystallinity obtained from Raman scattering, presented as I_c/I_a, was used as a major parameter to study the correlations between device performance and structural properties of μc-Si:H solar cells. Strong spatial non-uniformity of i-layer microstructure and device performance was revealed. It has been demonstrated that stable, high performance μc-Si:H solar cells can only be obtained with i-layers being μc-Si:H, yet close to the μc-Si:H to mixed-phase Si:H transition edge where an optimum micro-crystallinity range (I_c/I_a at around 1.8) was identified. Such optimum μc-Si:H solar cells exhibit moderate open-circuit voltages at ∼0.5 V, high fill factors, high efficiencies, and excellent stability against light-induced degradation. However, such optimum μc-Si:H i-layers demand a very narrow optimum processing window, which is probably the most critical challenge in developing low cost, large-scale μc-Si:H photovoltaic technology.

References

[1] A. Shah, J. Meier, E. Vallat-Sauvain, N. Wyrsch, U. Kroll, C. Droz, U. Graf, Sol. Cells 78 (2003) 469.
[2] O. Vetterl, F. Finger, R. Carius, P. Hapke, L. Houben, O. Kluth, A. Lambertz, A. Muck, B. Rech, H. Wagner, Sol. Cells 62 (2000) 97.
[3] K. Yamamoto, A. Nakajima, M. Yoshimi, T. Sawada, S. Fukuda, K. Hayashi, T. Suezaki, M. Ichikawa, Y. Koi, M. Goto, H. Takata, Y. Tawada, in: Conf. Record. 29th IEEE PVSC, 2002, p. 1110.
[4] K. Mori, T. Yasuda, M. Nishizawa, S. Yamasaki, K. Tanaka, Jpn. J. Appl. Phys. 39 (2000) 6647.
[5] Y. Nasuno, M. Kondo, A. Matsuda, Jpn. J. Appl. Phys. 40 (2001) L303.
[6] J. Bailat, E. Vallat-Sauvain, L. Feitknecht, C. Droz, A. Shah, J. Non-Cryst. Solids 299–302 (2002) 1219.
[7] S. Guha, J. Yang, D.L. Williamson, Y. Lubianiker, J.D. Cohen, A.H. Mahan, Appl. Phys. Lett. 74 (1999) 1860.
[8] Y.-M. Li, J.A. Anna Selvan, L. Li, R.A. Levy, A.E. Delahoy, in: Proc. 3rd WCPEC, 2003, p. 1788.
[9] B. Rech, T. Roschek, T. Repmann, J. Muller, R. Schmitz, W. Appenzeller, Thin Solid Films 427 (2003) 157.
[10] L. Li, Y.-M. Li, J.A. Anna Selvan, A.E. Delahoy, R.A. Levy, Mater. Res. Soc. Symp. Proc. 762 (2003) A5.15.1.
[11] R.W. Collins, A.S. Ferlauto, G.M. Ferreira, J. Koh, C. Chen, R.J. Koval, J.M. Pearce, C.R. Wronski, M.M. Al-Jassim, K.M. Jones, Mater. Res. Soc. Symp. Proc. 762 (2003) A10.1.1.
[12] F. Edelman, A. Chack, R. Weil, R. Beserman, Yu. L. Khait, P. Werner, B. Rech, T. Roschek, R. Carius, H. Wagner, W. Beyer, Sol. Cells 77 (2003) 125.
[13] A. Matsuda, K. Kumagai, K. Tanaka, Jpn. J. Appl. Phys. 22 (1982) L34.
[14] S. Veprek, Z. Iqbal, O. Kuhne, P. Capezzuto, F.A. Sarott, J.K. Gimzewski, J. Phys. C 16 (1983) 6241.
[15] K. Nakahata, A. Miida, T. Kamiya, Y. Maeda, C.M. Fortmann, I. Shimizu, Jpn. J. Appl. Phys. 37 (1998) L1026.
[16] E. Edelman, A. Chack, R. Weil, R. Beserman, Yu. L. Khait, P. Werner, B. Bech, T. Roschek, R. Carius, H. Wagner, W. Beyer, Sol. Cells 77 (2003) 125.
[17] M. Luysberg, C. Scholten, L. Houben, R. Carius, F. Finger, O. Vetterl, Mater. Res. Soc. Symp. Proc. 664 (2001) A 15.2.1.
[18] A.S. Ferlauto, R.J. Koval, C.R. Wronski, R.W. Collins, Appl. Phys. Lett. 80 (2002) 2666.
[19] C. Droz, E. Vallat-Sauvain, J. Bailat, L. Feitknecht, J. Meier, A. Shah, Sol. Energy Mater. Sol. Cells 81 (2004) 61.
[20] S. Kleim, F. Finger, R. Carius, T. Dylla, B. Rech, M. Grimm, L. Houben, M. Stutzmann, Thin Solid Films 430 (2003) 202.